Suspended sediment dynamics in a Southeast Asian mountainous catchment: Combining river monitoring and fallout radionuclide tracers

Elian Gourdin, O. Evrard, Sylvain Huon, Irene Lefevre, Olivier Ribolzi, Jean-Louis Reyss, Oloth Sengtaheuanghoung, Sophie Ayrault

1 Corresponding Author: Elian Gourdin

2 Telephone number: +33169824362

3 Email address: elian.gourdin@lsce.ipsl.fr

4

5 Title:

6 Suspended sediment dynamics in a Southeast Asian mountainous catchment: combining

7 river monitoring and fallout radionuclide tracers

8

Abstract

Soil erosion is intense in mountainous tropical regions where heavy storms result in the supply of large quantities of sediment to rivers. The origin and dynamics of suspended sediment were analysed in a catchment located in northern Laos during the first erosive flood of the rainy season in May 2012. The catchment was equipped with 4 successive gauging stations (draining areas ranging 0.2 - 11.6 km²). Fallout radionuclides (Beryllium-7 - ^{7}Be, unsupported Pb-210 -$^{210}Pb_{xs}$, and Cesium-137 -^{137}Cs) were determined on rainfall, overland flow, stream water, suspended sediment, soil surface and subsurface samples (with n = 3, 19, 75, 75, 65 and 14 respectively). Assumptions underpinning the ^{7}Be-labelling method were validated by implementing experiments in the laboratory (i.e., rainwater ^{7}Be sorption to soil particles) and in the field (i.e., ^{7}Be: $^{210}Pb_{xs}$ activity ratio evolution in rainwater and related overland flow during a natural storm event). Radionuclide analyses provided a way to quantify variations in sediment dynamics and origin throughout the flood: (1) a proportion of recently eroded sediment (labelled by ^{7}Be, and referred to as “fresh sediment”) ranging between *ca.* 8 - 35% in suspended loads; (2) higher contributions of fresh sediment at the beginning of the flood rising stage; (3) a progressive dilution of fresh sediment by particles remobilised from the riverbed / channel; (4) the dominance of particles originating from the soil surface (*ca.* 70 - 80% of total sediment load) in upper parts and a much larger contribution of subsurface material (*ca.* 64%) at the downstream station. The original contribution of ^{7}Be-labelled particles derived from collapsed riverbanks to sediment export was also demonstrated. This pilot study supports the use of fallout ^{7}Be and $^{210}Pb_{xs}$ in tropical catchments to constrain sediment dynamics. It also puts forward the need to better characterize the sources of sediment in order to avoid possible misinterpretations.

1. Introduction

Soil erosion is particularly intense in mountainous subtropical regions where heavy storms may result in the supply of large quantities of suspended sediment to streams (Descroix et al., 2008; Valentin et al., 2008). Large exports of suspended matter by mountain rivers lead to numerous problems downstream (Syvitski et al., 2005). Sediments can accumulate behind dams, which results in the siltation of water reservoirs (Downing et al., 2008; Thothong et al., 2011). Suspended matter also contributes to water quality degradation (Tanik et al., 1999) and conveys biological compounds, playing thereby a major role in global nutrient biogeochemical cycles (Quinton et al., 2010). It also constitutes a potential vector for various pollutants such as metals, polycyclic aromatic hydrocarbons or faecal bacteria (Ribolzi et al., 2010; Gateuille et al., 2014).

In order to limit those negative impacts, sediment supply to rivers needs to be controlled. Design and implementation of appropriate management procedures require a better understanding of suspended matter dynamics in mountainous catchments. Their behaviour should be better constrained in time, and particularly during floods, as most riverine sediments are exported during those short periods (Meybeck et al., 2003; Mano et al., 2009). To this end, tracers that are preferentially sorbed or contained in the fine mineral and organic suspended fractions (i.e., clays and fine silts, He and Walling, 1996) may be used to follow sediment pathways across catchments (Koiter et al., 2013).

Radionuclides that are supplied to the soil surface by rainfall, i.e. beryllium-7 (^{7}Be) and unsupported or excess lead-210 ($^{210}Pb_{xs}$) are used to estimate soil erosion rates at the hillslope scale (Schuller et al., 2006; Sepulveda et al., 2008), or to characterize the temporal transfer of sediment in larger river systems (Bonniwell et al., 1999). Their different half-lives ($T_{1/2}$ = 53 days for ^{7}Be and $T_{1/2}$ = 22.3 years for $^{210}Pb_{xs}$) are particularly relevant to differentiate between fresh sediment tagged with ^{7}Be and older remobilized sediment depleted in ^{7}Be. Based on this simple principle, Matisoff et al. (2005) proposed to calculate the ^{7}Be: $^{210}Pb_{xs}$ activity ratio ($^{7}Be/^{210}Pb_{xs}$) in both rainwater and riverine sediment to

estimate fresh sediment percentages in rivers and infer transfer times or transport distances. Alternative approaches used radionuclide mass-balance models such as the one proposed by Dominik et al. (1987) and improved by Le Cloarec et al. (2007), or associated both methods (Evrard et al., 2010). However, several limitations may arise regarding the assumptions underpinning those methods. The validity of radionuclides as tracers of sediment fluxes in large rivers has been recently questioned (Walling, 2012; Taylor et al., 2013). The main criticism focussed on the potential difference of $^{7}Be/^{210}Pb_{xs}$ activity ratio value in rainwater and in fresh sediment. This may occur when particles are tagged with radionuclides from successive storms and not with the event of investigation alone. Another concern arises from a possible misinterpretation of $^{7}Be/^{210}Pb_{xs}$ variations measured in sediment, as low values may result from various processes: radionuclide decay; desorption (when sediment remained buried in the riverbed) or changes in the source of sediment with the supply of subsurface particles (depleted in fallout radionuclides; e.g., Whiting et al., 2005). In order to reduce those uncertainties, a third fallout radionuclide, cesium-137 (^{137}Cs; $T_{1/2}$ = 30.2 years) proved to be useful to distinguish between particles originating from soil surface and exposed to atmospheric fallout of bomb tests during the second half of the 20th century (Ritchie and McHenry, 1990) and particles from the subsurface (below *ca.* 30 cm depth), protected from ^{137}Cs and ^{7}Be fallout (e.g. Olley et al., 1993; Ben Slimane et al., 2013; Evrard et al., 2013; Hancock et al., 2014).

In this study, experiments were carried out in the Houay Pano - Houay Xon nested catchments located in Laos and exposed to summer monsoon, to quantify the respective contributions of surface and subsurface soil to suspended sediment loads during an erosive flood event that took place at the beginning of the rainy season in May 2012. The fallout ^{7}Be activity of the previous rainy season should have sufficiently decayed during the 6-months dry period to become negligible compared to their recent supply at the onset of the wet season. Every compartment of the erosional system, from rainwater to stream

86 sediment, was sampled for fallout radionuclide analyses. Adsorption experiments were also
87 conducted for ^{7}Be at the microplot's scale under natural rainfall and in the laboratory.

88 2. Study site

89 The Houay Pano catchment, located 10 km south of Luang Prabang in northern Laos (Fig.
90 1), has been part of the MSEC (Monitoring Soil Erosion Consortium) network since 1998
91 (Valentin et al., 2008). The tropical monsoon climate of the region is characterized by the
92 succession of dry and wet seasons with *ca.* 80% of rainfall occurring during the rainy
93 season from May to October (Ribolzi et al., 2008). The Houay Pano stream has an average
94 base flow of 0.4 ± 0.1 L s^{-1} and is equipped with 2 gauging stations that subdivide the
95 catchment into nested subcatchments. These stations, S1 and S4, draining 20 ha and 60
96 ha respectively, are located along the main stem of the stream. Between S1 and S4
97 stations, water flows through a swamp (0.19 ha), supplied with water by a permanent
98 groundwater table (Fig. 1). Only temporary footslope and flood deposits can be found along
99 this narrow section of the stream and the swamp represents the major sediment
100 accumulation zone in the Houay Pano catchment. The Houay Pano stream flows into the
101 Houay Xon River (22.4 km² catchment) and is continuously monitored at S10 (draining a
102 11.6 km² catchment), located 2.8 km downstream of S4. The Houay Xon is a tributary of the
103 Nam Dong River, flowing into the Mekong River within the city of Luang Prabang (Ribolzi et
104 al., 2010).

105 The geological basement of the Houay Pano catchment is mainly composed of pelites,
106 sandstones and greywackes, overlaid in its uppermost part by Carboniferous to Permian
107 limestone cliffs. Soils consist of deep (>2 m) and moderately deep (>0.5 m) Alfisols
108 (UNESCO, 1974), except along crests and ridges where Inceptisols can be found (Chaplot
109 et al., 2009). Soils have a low cation exchange capacity and a low pH ranging between 4.9
110 –5.5 across the catchment. Native vegetation consisted of lowland forest dominated by
111 bamboos that were first cleared to implement shifting cultivation of upland rice at the end of

112 the 1960s (Huon et al., 2013). Elevation across the catchment ranges *ca.* 272–1300 m.a.s.l.
113 As cultivation takes place on steep slopes (ranging between 3-150%), the catchment is
114 prone to soil erosion (Chaplot et al., 2005; Ribolzi et al., 2011). Due to the decline of soil
115 productivity triggered by soil erosion over the years (Patin et al., 2012) and to an increasing
116 labour need to control weed invasion (Dupin et al., 2009), farmers progressively replaced
117 rice fields by teak plantations in the catchment (Fig. 1). During the present study, main land
118 uses in the Houay Pano catchment were teak plantations (36% of total area), rotating
119 cropping land (35%), Job's tears (10%), banana plantations (4%) and upland rice fields
120 (3%); the forest covering less than 9% of the area. The land use was different in the larger
121 area drained by S10, with 56% of the surface covered with forests, 15% under teak
122 plantations and 23% under cropland.

123 [Fig. 1]

124 3. Materials and methods

125 3.1. Sample and data collection

126 Rainfall, stream and overland flow waters were sampled during the May 23 flood in 2012.
127 Rainfall intensity was monitored with an automatic weather station (elevation: 536 m.a.s.l.)
128 and stream discharge was calculated from water level continuous recording and rating
129 curves. Rainfall was sampled with three cumulative collectors, located in the village near
130 the confluence between Houay Pano and Houay Xon streams, near a teak plantation on the
131 hillslopes located just upstream of the village and within the Houay Pano catchment.
132 Overland flow was collected at the outlet of 1-m^2 experimental plots. Stream water was
133 collected in plastic bottles after each 20-mm water level change by automatic samplers
134 installed at each gauging station. Fifty-six total suspended sediment (TSS) samples were
135 collected at the three stations (S1, S4, S10). Samples were dried shortly after collection in
136 an oven ($t \approx 100°C$) for 12-48 h. In addition, sediment deposited upstream of S4 in the river

channel (top 0-1 cm of in-channel deposits collected using a plastic trowel) was sampled the day before the May 23 flood to document the initial radionuclide activity. Surface soil samples (top 0–5 cm; n=65) were collected using plastic trowels on the hillslopes connected to the Houay Pano Stream and the Houay Xon River (Fig. 1) during three campaigns conducted in July 2002 (Huon et al., 2013), May 2012 and December 2012. Additional gully (n = 6) and riverbank (n = 8) samples were also collected in December 2012 to document the characteristics of the potential subsurface sources of sediment to the river.

Cumulative TSS exports were calculated at each station by summing the TSS masses exported between two successive sample collections. As no rating curve could be determined between TSS and Q (hysteresis patterns) during the entire event (absence of causal relationship between both parameters), TSS concentration was considered to vary linearly between successive measurements. Considering the relatively high number of successive samples collected at each station and the resulting high temporal resolution of TSS measurements, this assumption appeared to be reasonable. Sediment yields were calculated by dividing the cumulative TSS exports by the corresponding sub-catchment area.

3.2. Sample preparation and radionuclide analyses

To reduce the volume of rainwater (0.6 - 18 L) that would have been required to conduct direct gamma spectrometry analyses, fallout radionuclide recovery was performed in the field by co-precipitation with aluminium hydroxides (Ciffroy et al., 2003; Evrard et al., 2010). Samples were prepared by adding 1.5 g of aluminium chloride hexahydrate. Co-precipitation was achieved by addition of 1-N NaOH solution until pH attained 8.5-9.0. After 5 hours, the supernatant was removed and the precipitates were placed in an aluminium tray and dried in an oven. All residues were placed in polypropylene tubes and sealed airtight to contain ^{222}Rn and allow in-growth of its decay products. Counting was conducted

at the Laboratoire des Sciences du Climat et de l'Environnement (LSCE) in Gif-sur-Yvette by gamma spectrometry using a low-background, high-efficiency, well-type Ge detector with a crystal volume of 220 cm^3 (GWL-220-15 Ortec®). Most samples were analysed within less than 53 days (^{7}Be half-life) following the rainfall event.

Radionuclide activities were measured in a total of 45 individual or composite (depending on the quantity of material recovered) suspended sediment samples (0.2 – 15.1 g), 1 riverbed sediment sample (72 g) and 29 soil samples (48 – 78 g). Samples were packed into 15-60-ml (depending on the quantity available) polyethylene specimen cups and sealed airtight. The ^{7}Be, ^{137}Cs and ^{210}Pb activities were determined at 477.6 keV, 661.6 keV and 46.5 keV, respectively, by gamma spectrometry using the very low-background coaxial N- and P- type GeHP detectors (Canberra® and Ortec®) at LSCE. $^{210}Pb_{xs}$, was calculated by subtracting the supported activity from the total ^{210}Pb activity (measured at 46.5 keV) using two ^{226}Ra daughters, i.e. ^{214}Pb (average count at 295.2 and 351.9 keV) and ^{214}Bi (609.3 keV). When insufficient matter was available (<5 g), counting was performed with the same well-type Ge detector as for rainfall analyses. All measurements were corrected for background level determined every two months as well as for detector and geometry efficiencies. All results were expressed in Bq kg^{-1}. Activities were also decay corrected to the sampling date. Counting time reached a maximum of *ca.* 13 x 10^4 s for rainwater samples and *ca.* 25 x 10^4 s for soil and sediment samples, to optimize counting statistics. Counting efficiencies and reliability were conducted using internal and certified International Atomic Energy Agency (IAEA) standards prepared in the same specimen cups as the samples. Efficiencies were interpolated for ^{7}Be energy. Uncertainties on radionuclides activities were *ca.* 10% for $^{210}Pb_{xs}$, 20% for ^{7}Be and up to 30% for ^{137}Cs.

3.3. Estimates of fresh sediment (F) and surface soil (α) contributions to suspended loads

Respective proportions of (1) fresh sediment vs. particles isolated from recent fallout and, (2) surface soil -derived particles and subsurface particles (mobilized from gullies and

189 riverbanks) were estimated in TSS load. The fresh sediment proportion in TSS load was
190 estimated following the method (Eq. 1) proposed by Matisoff et al. (2005):

191 $F = 100 \times [(A/B) / (A_0/B_0)]$ (1)

192 where F is the percentage of fresh sediment, A and B are the ^{7}Be and $^{210}Pb_{xs}$ activities in
193 suspended sediment (Bq kg^{-1}) and A_0 and B_0 are the ^{7}Be and ^{210}Pb activities in rainfall (Bq
194 l^{-1}). Although the spatio-temporal variability of ^{7}Be and ^{210}Pb wet deposition may be
195 important for longer events or for successive storms, this study focused on a single event of
196 short duration and the use of a single value to characterize $^{7}Be/^{210}Pb$ in rainfall was shown
197 to be meaningful (Gourdin et al., 2014).

198 Proportion of surface soil -derived particles in a given sediment sample was estimated with
199 Eq. 2 (e.g., Brigham et al., 2001; Olley et al., 2012):

200 $\alpha = 100 \times [(Cs_{sample} - Cs_{subsurf.}) / (Cs_{surf.soil} - Cs_{subsurf.})]$ (2)

201 where α is the percentage of particles derived from surface soil, Cs_{sample} is the ^{137}Cs activity
202 in the sample, $Cs_{subsurf.}$ is the mean ^{137}Cs activity in the subsurface soils and $Cs_{surf.soil}$ is the
203 mean ^{137}Cs activity in the surface soils (top 0-2 cm).

204 3.4. Checking the field recovery procedure and the assumptions underpinning the ^{7}Be
205 method

206 In order to determine the efficiency and reproducibility of radionuclide recovery by co-
207 precipitation, experiments were carried out at LSCE. Six aliquots (2 L each) of rainwater
208 were prepared by adding aluminium chloride hexahydrate. Three of them were completely
209 evaporated using heating plates at 150°C for two days, assuming that 100% yields are
210 obtained by total evaporation (Cazala et al., 2003). Co-precipitation was conducted on the
211 three other aliquots using the procedure described in section 3.2. Supernatants were also

212 evaporated to determine the residual radionuclide activity that might still be present in the
213 solution after precipitation.

214 A simple experiment was carried out to assess ^{7}Be adsorption kinetics on soil particles
215 during rainfall. Five aliquots of a composite topsoil sample collected in the Houay Pano
216 catchment in Laos were mixed with rainwater (4.4 g L^{-1}) and centrifuged at high velocity
217 (25,000 rpm, *ca.* 78650 x g) using the Beckman Coulter® J-26 XP air-cooled centrifuge
218 facility at UMR Bioemco. The total contact time between soil particles and rainwater,
219 including acceleration and deceleration phases of the centrifuge, were 13, 23, 31, 41 and
220 72 min. After removal of supernatants, recovered sediments were evaporated and analysed
221 by gamma spectrometry as described in section 3.2.

222 In order to check the underlying assumption that fresh sediment labelling is characterized
223 by a $^{7}Be/^{210}Pb_{xs}$ similar to that of rainwater, ratios were compared in both rainfall and
224 overland flow water. To this end, overland flow and rainfall samples were collected
225 simultaneously at the outlet of a 1-m² experimental plot and of a *ca.* 8-m² rain-collector
226 during the June 1 rainfall event at the field site. The experiment was conducted on a fallow
227 soil with 33% slope and 60% vegetation cover (*ca.* 10 cm high). The rain collector was
228 installed at 1.8 m height from the soil surface to avoid splash contamination. Rainwater and
229 overland flow samples were collected in plastic bottles at the outlet of the plot and of the
230 rain collector. Radionuclide activities were determined in TSS samples dried in an oven,
231 and radionuclide recovery of rainfall samples was realized by co-precipitation as described
232 in section 3.2. Radionuclide stock variations for the experimental plot were calculated with 1
233 min- steps during the event using Eq. 3:

234 $$\Delta S_t = I_t - E_t \quad (3)$$

235 Where ΔS_t is the stock variation of the plot, I_t is the amount of radionuclide supplied by
236 rainfall to the plot and E_t is the amount of radionuclide exported from the plot by overland
237 flow, between time t-1 and time t (expressed in Bq m^{-2}).

238 3.5. Particle size distribution measurements

239 Particle size distribution (PSD) was analysed after a 48-h rehydration of TSS samples (≈1
240 g) in 50 mL of distilled water, followed by a 5-min immersion in a Branson 2510 ultrasonic
241 cleaning bath. We used the laser diffraction system (Malvern® Mastersizer 2000) coupled to
242 a liquid dispersing unit (Hydro 2000G) both available at the Earth Science Department
243 (University Paris-Sud, Orsay, France). As sediment samples were dried and rehydrated,
244 these PSD do not correspond to the "effective" PSD (Jouon et al., 2008). However, as no
245 dispersing agent was used, the distributions provided here also differ from "absolute" PSD.
246 The protocol was adjusted in order to ensure particle suspension without breaking all the
247 aggregates and allowing flocs' formation in the presence of organic matter, which is
248 assumed to occur naturally in the stream. Replicate measurements were realized to check
249 reproducibility (*ca.* ±0.5 µm), and the timing of analysis was adapted to optimize signal
250 stability. The PSD of each sample was obtained for 100 grain size classes ranging between
251 0.02 and 2000 µm. The parameter chosen for comparison between the particle size
252 distributions is d_{50}, corresponding to the median diameter of sediment particles (expressed
253 in µm) with 50% of total volume of particles in the sample below this grain size (e.g. Jouon
254 et al., 2008; Grangeon et al., 2012).

255 3.6. Water electrical conductivity measurement

256 In order to characterize stream / river baseflow dilution by storm event water, water
257 electrical conductivity was monitored every 6-min at the inlet of each gauging station using
258 Schlumberger in situ CTD probes, and additional measurements were conducted using an
259 YSI® 556 probe on each collected sample.

4. Results

4.1. Checking methodological assumptions

4.1.1. Radionuclide recovery procedure

Reproducibility and efficiency of fallout radionuclide recovery procedures used in this study are presented for ^{7}Be. Reproducibility was slightly better when conducting the total evaporation procedure (as described in Cazala et al., 2003), with a deviation of *ca.* 0.5% between triplicates, than when achieving co-precipitation (5% deviation). Differences induced by both treatments were lower than the 10% analytical uncertainty associated with ^{7}Be activities measured by gamma spectrometry. The recovery was equivalent for both co-precipitation (90 ± 6 mBq L^{-1}) and evaporation (86 ± 6 mBq L^{-1}) procedures. Activities measured in the supernatant (co-precipitation procedure) remained below the lower instrumental detection limits (<3% of co-precipitated sample activity) and a *ca.* 100% recovery of fallout radionuclides can therefore be assumed.

4.1.2. Fallout radionuclide adsorption kinetics

The adsorption kinetics experiment did not show any significant variation in ^{7}Be and $^{210}Pb_{xs}$ activity with time. The ^{7}Be activity in rainwater used in the experiment was 15 ± 2 Bq kg^{-1} and the initial ^{7}Be activity was null for soil particles. Mean activities of 10 ± 3 Bq kg^{-1} (range: 7 ± 2 to 13 ± 3 Bq kg^{-1}) for ^{7}Be and 29 ± 3 Bq kg^{-1} (range: 25 ± 4 to 32 ± 4 Bq kg^{-1}) for $^{210}Pb_{xs}$ were determined in particles. Taking into account all analytical uncertainties, total rainwater ^{7}Be adsorption was fulfilled at *ca.* 75-100% for all samples. The supply of $^{210}Pb_{xs}$ by rainfall (2.0 ± 0.2 Bq kg^{-1}) was low compared to its initial content in the soil (26 ± 2 Bq kg^{-1}). However, the activity in $^{210}Pb_{xs}$ measured in the soil after the experiment (28 ± 2 Bq kg^{-1}) remained consistent with the occurrence of additional sorption. Furthermore, ^{7}Be- and $^{210}Pb_{xs}$- sorption by soil particles occurred in less than 13 min, corresponding to the shortest contact time between water and soil particles that could be achieved during the experiment.

285 ^{7}Be and $^{210}Pb_{xs}$ labelling of soil particles by rainfall occurred very quickly as shown in other
286 studies (e.g. Taylor et al., 2012).

287 4.1.3. Fresh sediment labelling by rainfall

288 During the 1-m² plot experiment conducted on June 1, a 45 min- storm event with 11-mm
289 cumulative rainfall occurred. It triggered the export of 8.5 L of overland flow and 20 g of
290 fresh sediment. TSS samples (n = 13) were mixed together to form 3 successive composite
291 samples. Rainfall was characterised by activities ranging 57 - 171 ± 30 mBq L^{-1} for ^{7}Be and
292 37 - 166 ± 30 mBq L^{-1} for $^{210}Pb_{xs}$. Initial activities in surface soil (5 upper mm) collected on
293 May 31 before rainfall were 8 ± 1 Bq kg^{-1} for ^{7}Be and 60 ± 2 Bq kg^{-1} for $^{210}Pb_{xs}$. Overland
294 flow collected during rainfall displayed activities ranging 31 - 219 mBq L^{-1} for ^{7}Be and 11 -
295 345 mBq L^{-1} for $^{210}Pb_{xs}$. Related activities in suspended sediments ranged 24 - 95 ± 10 Bq
296 kg^{-1} for ^{7}Be and 10 - 100 ± 10 Bq kg^{-1} for $^{210}Pb_{xs}$. By comparison of radionuclide inputs and
297 exports (expressed in Bq m^{-2} min^{-1}) from the experimental plot, stocks of radionuclides were
298 calculated for each time step using Eq. 3. The evolutions of these stocks during each of the
299 45 minutes of the event are plotted versus the TSS concentration in the corresponding
300 overland flow exported from the experimental plot on Fig. 2.

301 [Fig. 2]

302 Stock variations were correlated with TSS concentration for ^{7}Be ($r^2 = 0.75$; Fig. 2a), $^{210}Pb_{xs}$
303 ($r^2 = 0.89$; Fig. 2b) and ^{137}Cs ($r^2 = 0.88$; Fig. 2c), confirming that radionuclides were
304 adsorbed by particles. Rainfall ^{7}Be and $^{210}Pb_{xs}$ inputs compensated the exports by TSS
305 loads below 2 g L^{-1} in the overland flow.Rainwater brought a total amount of 1.02 Bq m^{-2} for
306 ^{7}Be and 1.01 Bq m^{-2} for $^{210}Pb_{xs}$ (ratio: 1.0 ± 0.2). In the same time, overland flow exported
307 1.30 Bq m^{-2} for ^{7}Be and 1.59 Bq m^{-2} for $^{210}Pb_{xs}$ (ratio: 0.8 ± 0.2). Comparing total cumulative
308 inputs and exports, stock depletions were -0.27 Bq m^{-2}, -0.59 Bq m^{-2} and -0.02 Bq m^{-2}
309 during the event for ^{7}Be, $^{210}Pb_{xs}$ and ^{137}Cs, respectively. However, as no soil sample was

collected after the event, control of the stock balance could not be achieved. Overland flow particles F were estimated to 81 ± 20%, consistent with the assumption that freshly labelled sediments have $^{7}Be/^{210}Pb_{xs}$ similar to rainfall. Taking into account analytical errors associated with gamma - counting and their impact on $^{7}Be/^{210}Pb_{xs}$ estimates, this result strengthens the reliability of this ratio to fingerprint fresh sediment supply at the onset of the rainy season.

4.2. Application of the tracing method to a flood

4.2.1. Composition of potential sediment sources within the catchment

Mean radionuclide characteristics of surface soils, gullies and stream banks materials collected in the catchment are reported in Table 1.

[Table 1]

Surface and subsurface (stream banks and gullies) sources were best discriminated by their ^{137}Cs activity that is higher in surface soils. Mann-Whitney *U*-tests indicate statistically significant differences between surface and subsurface sources samples at $p<0.001$ for both ^{137}Cs and $^{210}Pb_{xs}$ activities.

4.2.2. Hydro-sedimentary characteristics of the May 23 flood

The particles exported during a flood at the onset of the rainy season 2012 in the Houay Xon catchment were collected successively all along the event at nested stations (Fig. 1) and analysed to investigate their sources and dynamics. The main characteristics of this event are described thereafter. The studied flood was triggered by a storm that occurred on May 23 2012 between 11:36 am and 12:24 pm. Rainfall intensity reached 85 mm h^{-1} between 11:54 am and 12:00 am, and cumulated 27 mm rainfall in 48 min. This event was below 0.01 y return period value (34.7 mm daily rainfall), according to Bricquet et al. (2003) for the 1950-2000 period. It was the first significant erosive event of the rainy season and

the first event with rainfall intensity exceeding 80 mm h^{-1}. Rainfall samples collected during the event displayed ^{7}Be activities ranging between 110 – 330 mBq L^{-1}. The main hydro-sedimentary characteristics of the flood are reported for the three gauging stations in Fig. 3-4-5.

[Fig. 3-4-5]

The lag time between stream discharge (Q) and rainfall intensity peaks differed at each station. Q increased 10 min after the rainfall peak and reached its maximum 10 min later at S1 (Fig. 3a), whereas at S4, Q rise started during the rainfall peak, and the Q peak occurred *ca.* 15 min later (Fig. 4a), i.e. 5 min before S1. This behaviour suggests an earlier beginning of rainfall on hillslopes located upstream of S4, with a progressive displacement of raincloud toward the location of the automatic weather station and the upstream S1 draining area (Fig. 1). Downstream at S10, the lag time between rainfall and Q peaks increased to 70 min (Fig. 5a). The evolution of TSS concentration as a function of stream discharge (Fig. 3b-4b-5b) displayed counterclockwise hysteresis dynamics (Williams, 1989) in the three subcatchments. Even though Q increased faster than TSS concentration at the beginning of the flood, water EC decreased concomitantly in the three stations (Fig. 3c-4c-5c). This evolution of stream EC suggests the progressive mixing of highly mineralized pre-event water (PEW, i.e. groundwater - high EC) with a low TSS concentration by weakly mineralized event water (EW, i.e. overland flow - low EC) with high sediment loads, the proportion of the EW increasing with decreasing EC (e.g., Nakamura, 1971; Pilgrim et al., 1979; Sklash and Farvolden, 1979; Ribolzi et al., 1997; Collins and Neal, 1998). Despite relatively common TSS-Q trends, major differences between the three stations were observed. At S1 the TSS maximum occurred 10 minutes after the water discharge peak and differed markedly between the water rising and recessing stages. During a second stage, TSS increased rapidly at the onset of Q decrease, reflecting the contribution of overland flow loaded with sediments originating from remote areas of the subcatchment.

During a third stage, TSS and Q decreased together. Station S4 showed the fastest response to rainfall. In contrast to S1, S4 displayed three discharge peaks. The first (and main) one likely corresponds to the contribution, upstream of the station, of hillslopes relatively close and well connected to the stream channel. The second and/or third peaks rather result from later arrival (at 12:55) of water flow originating from remote parts of the catchment (possibly including that exported from S1 30 min before). The evolution of Q *vs.* TSS during the rising and falling water stages followed relatively similar pathways (Fig. 4b). At S10, downstream of S4, Q increased with a time-lag of 22 min after the rainfall peak and the maximum Q was reached 45 min later. Two main successive water discharge peaks (12:42 and 13:17) were related to three successive TSS peaks (13:07, 13:33, 13:57; Fig. 5a), reflecting contributions to the river from distinct parts of the catchment. Each of the two first TSS peaks occurred *ca.* 30 min after the related Q peak. The first TSS peak (24 g L^{-1}) was recorded just before the second Q peak whereas the second and the third TSS peaks (respectively 25 and 22 g L^{-1}) occurred during the recessing stage, 22 and 27 min later.

Overall, high TSS concentrations (> 5 g L^{-1}) were maintained during the recession phase at the three monitoring stations. The amounts of sediment (calculated as described in section 3.1) exported from the three subcatchments are summarized in Table 2.

[Table 2]

Unfortunately, no sample was collected at the highest Q at S1. Therefore, these sediment exports and yields estimates (Table 2) could be slightly underestimated. The highest sediment yield was calculated at S4. It might be related to the larger area covered by teak plantations sensitive to soil erosion (32%) in this subcatchment, that is two-fold higher than in the drainage areas of S1 (14%) and S10 (15%). The river channel morphology and the hillslope-to-river connectivity varied across the area, as mentioned above in the description of hydro-sedimentary characteristics. The higher connectivity between cultivated hillslopes and the river upstream of S4 might also explain the higher sediment yield from this station.

386 4.2.3. Radionuclide measurements and estimates of fresh sediment (F) and surface-derived
387 particle (α) contributions

388 Rainfall activities ranged 0.11-0.33 Bq L^{-1} and 0.04-0.12 Bq L^{-1} for ^{7}Be and $^{210}Pb_{xs}$
389 respectively, with a mean $^{7}Be/^{210}Pb_{xs}$ of *ca*. 2.8. Weight fractions of fresh sediment were
390 calculated for all TSS samples using this latter value. As expected, ^{137}Cs was not detected
391 in rainfall. No ^{7}Be activity (<3 Bq kg^{-1}) could be determined for the deposited sediment
392 sample collected just before the flood (May 22) upstream S4 confirming the almost
393 complete decay of the previous year fallout.

394 At S1 and S4, ^{137}Cs activity in TSS increased with water discharge from *ca.* 1.0 Bq kg^{-1}
395 during the rising stage, then peaked near its maximum level (1.5-2.0 Bq kg^{-1}) and remained
396 nearly constant (*ca.* 1.5 ± 0.6 Bq kg^{-1}) during the falling stage period (Fig. 3e-4e). The
397 evolution was more variable at S10 (Fig. 5e). During the beginning of the rising stage, ^{137}Cs
398 activity in TSS was rather stable (*ca.* 0.8 ± 0.2 Bq kg^{-1}) with intermediate values between
399 surface soil signature and ^{137}Cs-depleted particles, found in gullies and stream banks
400 (Table 1). In contrast, $^{210}Pb_{xs}$ activities measured at S1, S4 and S10 (Fig. 3f-4f-5f) were
401 generally higher than the average level measured in catchment soils (*ca.* 40 Bq kg^{-1}, Table
402 1), in particular during the rising stage of the flood at S4. This little enrichment may result
403 from the preferential export of fine-grained particles – enriched in fallout radionuclides – by
404 overland flow (e.g., Walling and He, 1999; Matisoff, 2014). However, the values found in
405 TSS remained in the range of bulk surface soils $^{210}Pb_{xs}$ activities (up to 106 ± 3 Bq kg^{-1}).
406 Contrary to ^{137}Cs, ^{7}Be activities (and corresponding $^{7}Be/^{210}Pb_{xs}$) were higher during the
407 rising stage and then started to drop at peak flow maximum (Fig. 3g-4g-5g), following a
408 dilution pattern consistent with the behaviour of water EC (Fig. 3c-4c-5c). The overall trend
409 in S10 consisted in the mixing of: (i) particles with low ^{137}Cs activities – originating from
410 subsurface sources like collapsed riverbanks or deep rills / gully floor erosion (Hancock et
411 al., 2014) – but tagged with ^{7}Be and $^{210}Pb_{xs}$ supplied by recent rainfall and (ii) sediments

412 initially originating from surface soils with high ^{137}Cs but low ^{7}Be activities (which suggests
413 that they were immersed under water in deposition areas such as in swamps – see Huon et
414 al., 2013 – and isolated from recent fallout labelling before being resuspended during the
415 investigated flood).

416 A F value of *ca.* 10-30% was estimated during flood peaks and falling water stages (Fig. 3h-
417 4h-5h). Values in $^{7}Be/^{210}Pb_{xs}$ were not significantly different in most samples, except during
418 the beginning of the flood rise in S10, resulting in higher F (Fig. 5h). Those large analytical
419 uncertainties were either due to low sediment yields or to the short gamma counting time to
420 allow for analysing the entire sample set. However, proportional calculations show that
421 mixing of (1) 20-25% of fresh sediment originating from stream banks, depleted in ^{137}Cs
422 (*ca.* 0.4 Bq kg^{-1}, Table I), with (2) 75-80% of ^{137}Cs- labelled surface soil particles (*ca.* 2.2 Bq
423 kg^{-1}, Table I), would provide estimates of *ca.* 1.8 Bq kg^{-1}, consistent with the ^{137}Cs activities
424 measured in TSS at S1 and S4 (Fig. 3e-4e). The contribution of fresh sediment was more
425 important at S10, up to *ca.* 35% at the beginning of the flood (20% of TSS export during the
426 flood). At S1 and S4, ^{7}Be activities (in Bq L^{-1}) were positively correlated with TSS
427 concentrations (r^2 = 0.85 and 0.88, respectively; Fig. 6a-6b) during the entire flood. This
428 behaviour confirms that ^{7}Be is transported by the solid phase in the stream samples of the
429 Houay Pano upstream catchment. However, for S10, no clear trend was observed on a
430 similar plot (not shown). Furthermore, ^{7}Be activities in TSS (in Bq kg^{-1}; Fig. 5g) decrease
431 when TSS loads increase (Fig. 5a). This trend reflects that particles tagged with ^{7}Be that
432 are exported from S10 at the beginning of the flood are then diluted by ^{7}Be-depleted TSS
433 loads, which highlights a different behaviour in the downstream part of the Houay Xon
434 catchment compared with upstream stations of the Houay Pano subcatchment.

435 [Fig. 6]

436 Results obtained at S10 suggest a mixing between a ^{7}Be-labelled source of fresh sediment
437 and remobilized sediment from the river channel. In addition, variations in the origin of

suspended sediment were observed at this station. Mean ^{137}Cs activity measured at S10 (*ca.* 1.0 Bq kg^{-1}) was lower than at S1 (1.4 Bq kg^{-1}) and S4 (1.6 Bq kg^{-1}), revealing a larger contribution of particles originating from subsurface sources at this station, which is consistent with our field observations. Vegetated riverbanks are less sensitive to erosion upstream of S4 where the stream bed does not deeply incise the bedrock. Using Eq. 2 (section 3.3), we estimated a contribution of *ca.* 90% of ^{137}Cs-depleted sediment at the beginning of the flood at S10. A potential explanation would be that those particles were initially supplied to the river by stream bank erosion or collapse during the former wet season(s). At the end of the previous rainy season, i.e. 6 months before the studied flood, this sediment was deposited in the river channel. As the river level decreased during the dry season, subsequent exposure to atmospheric fallout took place at the beginning of the wet season. The morphology of the riverbed upstream of S10 is consistent with the formation of such deposits. The remainder of sediments depleted in both ^{137}Cs and ^{7}Be were likely "older" particles originating from riverbanks or gullies and deposited in the river channel during the previous years. Furthermore, when plotting estimated F and α for S10, nearly all data points (except 2) are aligned (Fig. 6c). The two outlying samples correspond to the first and the third TSS peaks, which are likely associated with the export of material with a different origin, suggesting the contribution of a third type of source. Both samples are located below the regression line, reflecting their depletion in fallout radionuclides, which suggests that they were supplied by deep gully walls or riverbank erosion processes (Olley et al., 1993, 2012; Hancock et al., 2014) that were not dominant during the rest of the event. When excluding those two samples implying this third secondary source, a negative linear correlation (r^2=0.97; Fig. 6c) is observed during the flood. High contributions of fresh sediment are associated with exports of particles originating from subsurface soils, whereas remobilized sediments are mainly originating from surface soils. This observation outlines the existence of a source of fresh sediment, derived from collapsed riverbanks, that represents a significant proportion of the TSS load conveyed at this station.

465 4.2.4. Particle size distribution of suspended sediments

466 The relationship between TSS grain size and water discharge was investigated by
467 comparing d_{50} (median particle size) values for the three stations (Fig. 3d-4d-5d). The
468 lowest d_{50} value (4 µm) was recorded at S4 at the end of the flood whereas, the highest
469 value (12 µm) was measured during the discharge maximum at S10. Mean d_{50} at S1, S4
470 and S10 reached 6.3, 6.9 and 8.1 µm, respectively, reflecting the increasing discharge and
471 the higher competence of the river in downstream direction.

472 All three stations presented high d_{50} during the peaks of discharge that corresponded to the
473 transport of both freshly eroded and remobilized particles. During the recessing stage of the
474 flood, transport was progressively replaced by deposition of particles on the streambed, as
475 d_{50} decreased to 5, 5.5 and 6 µm at S1, S4 and S10 respectively.

476 5. Discussion

477 5.1. Sediment sources and dynamics along the river continuum

478 The time-lag between water and sediment peaks observed at S10 may result from the
479 presence of a dense vegetation cover on both riverbed and banks that represent obstacles
480 to flow propagation (Gurnell, 2007). Although it did not stop completely the transport of
481 upstream particles as the discharge was high, it may have slowed them down and delayed
482 their arrival compared to water flow propagation, by increasing Houay Xon River channel
483 hydraulic roughness (Manning, 1889) in a similar way as the so-called “grassed waterways”
484 (GWW) installed in agricultural lands to combat muddy runoff generated on cultivated
485 hillslopes (Evrard et al., 2008). Furthermore, this effect should increase with the distance of
486 transportation (Heidel, 1956) as S4 sediment exports had to travel approximately 3 km
487 before reaching S10. As reported by Williams (1989), such counterclockwise hysteresis
488 dynamics may occur in highly erodible catchments submitted to prolonged erosion. Similar
489 lagging sediment peaks were also observed in larger catchments receiving the successive

contributions from areas characterized by low and high specific sediment yields (Yun-Liang et al., 1985). Inversely, Whiting et al. (2005) reported clockwise hysteresis dynamics for suspended sediment concentration and fallout radionuclide activity (in Bq L^{-1}) recorded at successive stations along the Yellowstone River (samples collected during seven different floods between April and July 2000). Smith and Dragovitch (2009) reported several counterclockwise hysteresis events at the upstream station of nested catchments affected by severe gully and riverbank erosion in south-eastern Australia's uplands. However, clockwise hysteresis patterns were mostly observed in these catchments, and they were interpreted as resulting from sediment exhaustion effects, particularly during multi-rise events.

[Fig. 7]

The changes in suspended sediment signatures during the flood at the upstream stations (S1 and S4; Fig. 7a-b) indicate that they were mostly derived from surface soils (tagged by 20^{th} century ^{137}Cs fallout), which is consistent with previous observations made in the Houay Pano catchment (Huon et al., 2013). Previous works by Chaplot et al. (2005) reported the formation of gullies and rills on hillslopes upstream of S4 and S1 in 2001. However, most of those linear features formed during a rainfall event of higher intensity (90 mm cumulative rainfall; return period > 2 yrs). This storm took place in August, i.e. at the period of the rainy season with the lowest infiltrability and highest mean monthly rainfall (Patin et al., 2012). During the 23 May 2012 event, no active gully was observed in the field. Furthermore, we could not quantify specifically the contribution of rill erosion to sediment exports for this event (Evrard et al., 2010; Ben Slimane et al., 2013). Nevertheless, suspended material conveyed at the downstream station contained lower ^{137}Cs activities (Fig. 5e), suggesting a switch in the source of particles at this scale with the likely contribution of collapsed riverbanks (e.g. Nagle and Ritchie, 2004). Decreasing ^{137}Cs fluxes with increasing drainage areas had been previously reported by Whiting et al. (2005) and

516 interpreted as resulting from bank erosion increase in downstream direction. These authors
517 also reported the dominance of new sediment at upstream stations and early in the
518 hydrograph. Indeed, the global trend observed at S10 (Fig. 7c) corresponded to the arrival,
519 at the beginning of the flood, of particles from collapsed riverbanks originating from the
520 Houay Xon River channel section, associated with a first peak of discharge. Then, during
521 the main discharge peak, more particles mobilized from remote surface soils by overland
522 flow were exported. Those materials were mixed with remobilized sediment from the river
523 channel that diluted the fresh sediment input signal. Finally, as Q decreased, remobilized
524 and eroded particles from most remote sources were exported and progressively deposited.

525 Cumulative exports of fresh sediment were estimated to *ca.* 0.3, 3 and 26 Mg for S1, S4
526 and S10, respectively. They represented respectively *ca.* 13, 12 and 20% of the total
527 suspended sediment exports previously estimated (see section 4.2.2; Table 2).
528 Corresponding estimates in individual suspended sediment samples ranged *ca.* 10 - 60% of
529 surface soil-derived particles. Furthermore, the mean contribution of surface-derived
530 particles was estimated to *ca.* 60 and 76% at S1 and S4, respectively, whereas it amounted
531 to only 29% at S10, reflecting the importance of subsurface sources contribution
532 downstream of S4 (Fig. 7).

533 5.2. Methodological assumptions and prospects

534 Due to the absence of pre-event ^{7}Be labelling (Appendix) the May 23 flood event appeared
535 to be the first major erosive flood of the 2012 rainy season. Therefore, the hypotheses
536 underpinning the use of the $^{7}Be/^{210}Pb_{xs}$ method (Matisoff et al., 2005; Schuller et al., 2006)
537 were simplified. At the plot scale, $^{7}Be/^{210}Pb_{xs}$ in rainwater and fresh sediment showed a
538 strong similarity during a comparable storm to that of May 23. As this study focused on a
539 single event of short duration (*ca.* 1h rainfall with 60% total cumulative water depth in 12
540 min) the use of a single integrated value for rainfall $^{7}Be/^{210}Pb_{xs}$ proved to be meaningful.
541 However, for longer lasting events, progressive decrease of radionuclide content in

542 rainwater may occur (Wallbrink and Murray, 1994; Ioannidou and Papastefanou, 2006;
543 Gourdin et al., 2014). In order to estimate radionuclide signature of fresh sediment inputs to
544 the rivers, overland flow could be collected and analysed instead of rainfall. Indeed, as
545 showed by Chaplot and Poesen (2012), only a limited proportion of soil-detached (and
546 freshly ^{7}Be-labelled) particles may reach the Houay Pano stream channel and be
547 transported downstream. The transport of those particles by overland flow progressively
548 decreased with rainfall intensity and most of mobilized materials were deposited and
549 remained on hillslopes. Comparable conclusions could be drawn from soil ^{137}Cs inventories
550 (Huon et al., 2013). This behavior may be responsible for the global trend to progressive
551 decrease of ^{7}Be activity in TSS observed at all stations during the event.

552 Studies investigating $^{7}Be/^{210}Pb_{xs}$ variations in catchments and rivers grew in number during
553 the last years (Taylor et al., 2013). However, they were conducted over a wide range of
554 time (1h–1yr) and spatial scales (0.7–390 km²) for different environmental and climatic
555 contexts, and their results may not be easy to compare to our study. The main $^{7}Be/^{210}Pb_{xs}$
556 values and related F estimates found in the literature are summarized in Table 3.

557 [Table 3]

558 A large seasonal variability was observed for these ratios depending, among other factors,
559 on the origin of air masses evolving throughout the year and across regions (Bourcier et al.,
560 2011). We could, nevertheless, compare our results with those obtained for a composite
561 sediment sample collected during the first erosive flood of the rainy season in central
562 Mexico (Evrard et al., 2010) where similar conditions prevailed. A comparable contribution
563 of fresh sediment (*ca.* 25 ± 4%) was supplied to the stream, suggesting the dominance (75–
564 87%) of processes remobilizing “older” material at the beginning of the wet season.
565 However in both cases, more detailed spatial information is needed to characterize the
566 origin (surface vs. subsurface) of both freshly eroded and remobilized sediment. In this
567 study, we could determine the sources supplying suspended sediment (mainly derived from

surface soils) during this early monsoon event and constrain their dynamics. The bulk of exported particles was remobilized from previous year deposits accumulated in the stream/river channel system.

The chosen nested approach provided a way to outline changes in the succession of dominant processes along the river system, from headwaters to the outlet with contrasting sensitivities to erosion along the stream path (Table 2) and a variable connectivity between hillslopes and the main river channel. Whilst hillslopes were directly connected to the stream in upper parts of the catchment, the connection between surface sources and the Houay Xon River was less direct in the downstream sections, characterized by a gentler topography and the presence of depositional areas including a swamp and a wider river channel. Furthermore, the variations in land uses and covers characterized by varying sensitivities to erosion observed across the catchment also partly explain the differences in sediment yields calculated in the drainage areas of the 3 stations. The higher sediment yields calculated at S4 might therefore be explained by the presence of well-connected hillslopes covered by teak plantations. Indeed, this particular land use has been detected as generating large quantities of runoff, especially when teak age exceeds 10 years (Patin et al., 2012).

Our results suggest that information on sediment sources (i.e., surface vs. subsurface) should be systematically provided when using $^{7}Be/^{210}Pb_{xs}$ to avoid misinterpretations on their variations. Furthermore, given the rather large uncertainties associated with their results due to logistical and analytical constrains that are difficult to reduce, interpretation of these ratios should remain cautious (e.g. by mentioning proportions of fresh sediment instead of sediment ages in days). It should also focus on the identification of sources and processes of sediment export during the main flood stages. Under those conditions, the $^{7}Be/^{210}Pb_{xs}$ method will provide useful constrains on the processes controlling sediment

593 dynamics in rivers and support design and implementation of efficient soil conservation
594 measures to limit erosion.

595 6. Conclusions

596 An early monsoon flood was monitored at three nested stations in the Houay Xon
597 catchment (Laos) and suspended sediment content in fallout radionuclides was analysed
598 throughout the event. Our results showed that rainwater fallout radionuclides were quickly
599 (< 13 min) bound to surface soil particles. Furthermore, freshly mobilized sediments in
600 overland flow displayed a $^{7}Be/^{210}Pb_{xs}$ similar to the one measured in rainwater.

601 Consequently, fresh sediment contributions were estimated for each of the three nested
602 sub-catchments. During this first erosive flood of the rainy season, remobilized particles
603 represented the main type of sediment exported, whatever the spatial scale considered.
604 Contribution of sediments originating from surface soils was dominant upstream (69-78%)
605 whereas they only represented 36% of suspended load downstream, highlighting the key
606 role played by land use and hill slope connectivity on sediment delivery to the river in the
607 different subcatchments.

608 Furthermore, fallout radionuclides provided a mean to identify the contribution of ^{7}Be-
609 labelled particles originating from collapsed riverbank sediments, deposited on aerial
610 exposed areas in the river channel.

611 This study highlights the interest of combining $^{7}Be/^{210}Pb_{xs}$ measurements with additional
612 parameters providing information on sediment origin in order to avoid misinterpretation of
613 their dynamics. Further work should attempt to use similar combinations of tracers applied
614 to a longer river continuum (integrating more or larger nested subcatchments). Tracking the
615 downstream flood propagation would provide an opportunity to outline the evolution of
616 dominant processes and sources in larger mountainous tropical catchments where
617 excessive erosion results in critical problems. Providing such information appears crucial to

design efficient conservation measures in upstream catchments to prevent an excessive supply of sediment to the rivers.

Acknowledgements

The authors would like to thank the Lao NAFRI (National Agriculture and Forestry Research Institute in Vientiane) and the MSEC project (Multi-Scale Environment Changes) for their support. They are also grateful to Keo Oudone Latsachack, Bounsamai Soulileuth and Chanthamousone Thammahacksa for their kind, constant and irreplaceable help in the field and to Christophe Colin and Olivier Dufaure for their help to organize and conduct the Particle Size Distribution measurements. Elian Gourdin received a PhD fellowship from Paris-Sud University. This work received financial support from the French CNRS EC2CO / BIOHEFECT programme (Belcrue project). Finally, the authors would like to thank the three anonymous reviewers, whose comments helped to improve the manuscript.

7. References

Ben Slimane, A., Raclot, D., Evrard, O., Sanaa, M., Lefèvre, I., Ahmadi, M., Tounsi, M., Rumpel, C., Ben Mammou, A., Le Bissonnais, Y. (2013). Fingerprinting sediment sources in the outlet reservoir of a hilly cultivated catchment in Tunisia. *Journal of Soils and Sediments*, 13(4), 801–815.

Bonniwell, E. C., Matisoff, G., Whiting, P. J. (1999). Determining the times and distances of particle transit in a mountain stream using fallout radionuclides. *Geomorphology*, 27, 75–92.

Bourcier, L., Masson, O., Laj, P., Pichon, J. M., Paulat, P., Freney, E., Sellegri, K. (2011). Comparative trends and seasonal variation of ^{7}Be, ^{210}Pb and ^{137}Cs at two altitude sites in the central part of France. *Journal of Environmental Radioactivity*, 102(3), 294–301.

Bricquet, J.-P., Boonsaner, A., Bouahom, B., Toan, T. D. (2003). Statistical Analysis of Long Series Rainfall Data: A Regional Study in South-East Asia. In A. R. Maglinao, C. Valentin, F. Penning de Vries (Eds.), *From soil research to land and water management: harmonizing people and nature: proceedings of the IWMI-ADB project annual meeting and 7th MSEC assembly. Vientiane (LAO).* (pp. 83–89). Vientiane (LAO): IWMI-ADB Project Annual Meeting; MSEC Assembly, 7.

Brigham, M.E., McCullough, C.J., Wilkinson, P. (2001). Analysis of suspended-sediment concentrations and radioisotope levels in the Wild River Basin, Northwest Minnesota, 1973–98. *U.S. Geological Survey Water- Resources Investigations Report 01-4192*, 21 p.

651 Cazala, C., Reyss, J. L., Decossas, J. L., Royer, A. (2003). Improvement in the
652 determination of ^{238}U, $^{228-234}Th$, $^{226-228}Ra$, ^{210}Pb, and ^{7}Be by gamma spectrometry on
653 evaporated fresh water samples. *Environmental Science and Technology*, 37(21),
654 4990–4993.

655 Chaplot, V, Coadoulebrozec, E., Silvera, N., Valentin, C. (2005). Spatial and temporal
656 assessment of linear erosion in catchments under sloping lands of northern Laos.
657 *Catena*, 63(2-3), 167–184.

658 Chaplot, V., Podwojewski, P., Phachomphon, K., Valentin, C. (2009). Soil Erosion Impact
659 on Soil Organic Carbon Spatial Variability on Steep Tropical Slopes. *Soil Science*
660 *Society of America Journal*, 73(3), 769.

661 Chaplot, V., Poesen, J. (2012). Sediment, soil organic carbon and runoff delivery at various
662 spatial scales. *Catena*, 88(1), 46–56.

663 Ciffroy, P., Reyss, J. L., Siclet, F. (2003). Determination of the residence time of suspended
664 particles in the turbidity maximum of the Loire estuary by ^{7}Be analysis. *Estuarine,*
665 *Coastal and Shelf Science*, 57(4), 553–568.

666 Collins, R.U., Neal, C. (1998). The hydrochemical impacts of terraced agriculture , Nepal.
667 *Science of the Total Environment,* 212, 233–243.

668 Descroix, L., González Barrios, J. L., Viramontes, D., Poulenard, J., Anaya, E., Esteves, M.,
669 Estrada, J. (2008). Gully and sheet erosion on subtropical mountain slopes: Their
670 respective roles and the scale effect. *Catena*, 72(3), 325–339.

671 Dominik, J., Burrus, D., Vernet, J.-P. (1987). Transport of the environmental radionuclides
672 in an alpine watershed. *Earth and Planetary Science Letters*, 84(2–3), 165–180.

673 Downing, J. A., Cole, J. J., Middelburg, J. J., Striegl, R. G., Duarte, C. M., Kortelainen, P.,
674 Prairie, Y. T., Laube, K. A. (2008). Sediment organic carbon burial in agriculturally
675 eutrophic impoundments over the last century. *Global Biogeochemical Cycles*, 22(1),
676 1–10.

677 Dupin, B., de Rouw, A., Phantahvong, K. B., Valentin, C. (2009). Assessment of tillage
678 erosion rates on steep slopes in northern Laos. *Soil and Tillage Research*, 103(1), 119–
679 126.

680 Evrard, O., Vandaele, K., van Wesemael, B., Bielders, C.L. (2008). A grassed waterway
681 and earthen dams to control muddy floods from a cultivated catchment of the Belgian
682 loess belt. *Geomorphology,* 100(3-4), 419–428.

683 Evrard, O., Némery, J., Gratiot, N., Duvert, C., Ayrault, S., Lefèvre, I., Poulenard, J., Prat,
684 C., Bonté, P., Esteves, M. (2010). Sediment dynamics during the rainy season in
685 tropical highland catchments of central Mexico using fallout radionuclides.
686 *Geomorphology*, 124(1-2), 42–54.

687 Evrard, O., Poulenard, J., Némery, J., Ayrault, S., Gratiot, N., Duvert, C., Prat, C., Lefèvre,
688 I., Bonté, P., Esteves, M. (2013). Tracing sediment sources in a tropical highland
689 catchment of central Mexico by using conventional and alternative fingerprinting
690 methods. *Hydrological Processes*, 27(6), 911–922.

691 Gateuille, D., Evrard, O., Lefèvre, I., Moreau-Guigon, E., Alliot, F., Chevreuil, M., Mouchel,
692 J.-M. (2014). Mass balance and depollution times of Polycyclic Aromatic Hydrocarbons
693 in rural nested catchments of an early industrialized region (Orgeval River, Seine River
694 basin, France). *Science of the Total Environment*, 470-471, 608-617.

695 Gourdin, E., Evrard, O., Huon, S., Reyss, J.-L., Ribolzi, O., Bariac, T., Sengtaheuanghoung,
696 O., Ayrault, S. (2014). Spatial and temporal variability of ^{7}Be and ^{210}Pb wet deposition
697 during four successive monsoon storms in a catchment of northern Laos. *Journal of*
698 *Environmental Radioactivity,* 136, 195–205.

699 Grangeon, T., Legout, C., Esteves, M., Gratiot, N., Navratil, O. (2012). Variability of the
700 particle size of suspended sediment during highly concentrated flood events in a small
701 mountainous catchment. *Journal of Soils and Sediments*, 12(10), 1549–1558.

702 Gurnell, A. M. (2007). Analogies between mineral sediment and vegetative particle
703 dynamics in fluvial systems. *Geomorphology*, 89(1-2), 9–22.

704 Hancock, G. J., Wilkinson, S. N., Hawdon, A. A., Keen, R. J. (2014). Use of fallout tracers
705 ^{7}Be, ^{210}Pb and ^{137}Cs to distinguish the form of sub-surface soil erosion delivering
706 sediment to rivers in large catchments. *Hydrological Processes,* 28, 3855–3874.

707 He, Q., Walling, D. E. (1996). Interpreting particle size effects in the adsorption of ^{137}Cs and
708 unsupported ^{210}Pb by mineral soils and sediments. *Journal of Environmental*
709 *Radioactivity,* 30(2), 117–137.

710 Heidel, S. G. (1956). The progressive lag of sediment concentration with flood waves.
711 *Trans. Am. Geophys. Union*, 37(1), 56–66.

712 Huisman, N. L. H., Karthikeyan, K. G., Lamba, J., Thompson, A. M., Peaslee, G. (2013).
713 Quantification of seasonal sediment and phosphorus transport dynamics in an
714 agricultural watershed using radiometric fingerprinting techniques. *Journal of Soils and*
715 *Sediments*, 13(10), 1724-1734.

716 Huon, S., de Rouw, A., Bonté, P., Robain, H., Valentin, C., Lefèvre, I., Girardin, C., Le
717 Troquer, Y., Podwojewski, P., Sengtaheuanghoung O. (2013). Long-term soil carbon
718 loss and accumulation in a catchment following the conversion of forest to arable land
719 in northern Laos. *Agriculture, Ecosystems and Environment*, 169, 43–57.

720 Ioannidou, A, Papastefanou, C. (2006). Precipitation scavenging of ^{7}Be and ^{137}Cs
721 radionuclides in air. *Journal of Environmental Radioactivity*, 85(1), 121–36.

722 Koiter, A. J., Owens, P. N., Petticrew, E. L., Lobb, D. A. (2013). The Behavioural
723 Characteristics of Sediment Properties and their Implications for Sediment
724 Fingerprinting as an Approach for Identifying Sediment Sources in River Basins. *Earth-*
725 *Science Reviews*, 125, 24–42.

726 Le Cloarec, M.-F., Bonté, P., Lefèvre, I., Mouchel, J.-M., Colbert, S. (2007). Distribution of
727 ^{7}Be, ^{210}Pb and ^{137}Cs in watersheds of different scales in the Seine River basin:
728 Inventories and residence times. *Science of the Total Environment*, 375(1–3), 125–139.

729 Manning, R. (1889). On the flow of water in open channels and pipes. *Trans. Inst. Civ. Eng.*
730 *Ireland*, 20, 161–207.

731 Mano, V., Nemery, J., Belleudy, P., Poirel, A. (2009). Assessment of suspended sediment
732 transport in four Alpine watersheds (France): influence of the climatic regime.
733 *Hydrological Processes*, (23), 777–792.

734 Matisoff, G. (2014). ^{210}Pb as a tracer of soil erosion, sediment source area identification and
735 particle transport in the terrestrial environment. *Journal of Environmental Radioactivity,*
736 *in press.*

737 Matisoff, G., Wilson, C. G., Whiting, P. J. (2005). The ^{7}Be/^{210}Pb$_{xs}$ ratio as an indicator of
738 suspended sediment age or fraction new sediment in suspension. *Earth Surface*
739 *Processes and Landforms*, 30(9), 1191–1201.

740 Meybeck, M., Laroche, L., Dürr, H. H., Syvitski, J. P. M. (2003). Global variability of daily
741 total suspended solids and their fluxes in rivers. *Global and Planetary Change*, 39(1-2),
742 65–93.

743 Nagle, G. N., Ritchie, J. C. (2004). Wheat field erosion rates and channel bottom sediment
744 sources in an intensively cropped northeastern Oregon drainage basin. *Land*
745 *Degradation and Development*, 15(1), 15–26.

746 Nakamura, R. (1971). Runoff analysis by electrical conductance of water. *Journal of*
747 *Hydrology,* 14, 197–212.

748 Olley, J. M., Murray, A. S., Mackenzie, D. H., Edwards, K. (1993). Identifying sediment
749 sources in a gullied catchment using natural and anthropogenic radioactivity. *Water*
750 *Resources Research*, 29(4), 1037–1043.

751 Olley, J., Burton, J., Smolders, K., Pantus, F., Pietsch, T. (2012). The application of fallout
752 radionuclides to determine the dominant erosion process in water supply catchments of
753 subtropical South-east Queensland, Australia. *Hydrological Processes*, 27(6), 885–895.

754 Patin, J., Mouche, E., Ribolzi, O., Chaplot, V., Sengtahevanghoung, O., Latsachak, K. O.,
755 Soulileuth, B., Valentin, C. (2012). Analysis of runoff production at the plot scale during
756 a long-term survey of a small agricultural catchment in Lao PDR. *Journal of Hydrology*,
757 426-427, 79–92.

758 Pilgrim, D.H., Huff, D.D., Steele, T.D. (1979). Use of specific conductance and contact time
759 relations for separating flow components in storm runoff. *Water Resources Research,*
760 15, 329–339.

761 Quinton, J. N., Govers, G., Van Oost, K., Bardgett, R. D. (2010). The impact of agricultural
762 soil erosion on biogeochemical cycling. *Nature Geoscience*, 3(5), 311–314.

763 Ribolzi, O., Moussa, R., Gaudu, J.-C., Vallès, V., Voltz, M. (1997). Etude des crues de
764 transition entre période sèche et période humide, par traçage naturel sur un bassin
765 versant méditerranéen cultivé. *Comptes Rendus Geosci.* 324, 985–992.

766 Ribolzi, O., Cuny, J., Sengsoulichanh, P., Pierret, A., Thiébaux, J. P., Huon, S., Bourdon,
767 E., Robain, E., Sengtaheuanghoung O. (2008). Assessment of water quality along a
768 tributary of the Mekong River in a mountainous, mixed land-use environment of the Lao
769 P.D.R. *The Lao Journal of Agriculture and Forestry*, (17), 91–111.

770 Ribolzi, O., Cuny, J., Sengsoulichanh, P., Mousquès, C., Soulileuth, B., Pierret, A., Huon,
771 S., Sengtaheuanghoung O. (2010). Land use and water quality along a Mekong
772 tributary in northern Lao P.D.R. *Environmental management*, 47(2), 291–302.

773 Ribolzi, O., Patin, J., Bresson, L. M., Latsachack, K. O., Mouche, E., Sengtaheuanghoung,
774 O., Silvera, N.,Thiébaux, J. P., Valentin, C. (2011). Impact of slope gradient on soil
775 surface features and infiltration on steep slopes in northern Laos. *Geomorphology*, 127,
776 53–63.

777 Schuller, P., Iroumé, A., Walling, D. E., Mancilla, H. B., Castillo, A., Trumper, R. E. (2006).
778 Use of Beryllium-7 to Document Soil Redistribution following Forest Harvest
779 Operations. *Journal of Environmental Quality*, 35, 1756–1763.

780 Sepulveda, A., Schuller, P., Walling, D. E., Castillo, A. (2008). Use of ^{7}Be to document soil
781 erosion associated with a short period of extreme rainfall. *Journal of environmental*
782 *radioactivity*, 99(1), 35–49.

783 Sklash, M.G., Farvolden, R.N. (1979). The role of groundwater in storm runoff. *Journal of*
784 *Hydrology,* 43, 45–65.

785 Smith, H.G., Dragovich, D. (2009). Interpreting sediment delivery processes using
786 suspended sediment-discharge hysteresis patterns from nested upland catchments,
787 south-eastern Australia. *Hydrological Processes*, 23, 2415–2426.

788 Syvitski, J. P. M., Vörösmarty, C. J., Kettner, A. J., Green, P. (2005). Impact of humans on
789 the flux of terrestrial sediment to the global coastal ocean. *Science* 308(5720), 376–80.

790 Tanik, A., Beler Baykal, B., Gonenc, I. E. (1999). The impact of agricultural pollutants in six
791 drinking water reservoirs. *Water Science and Technology*, 40(2), 11–17.

792 Taylor, A., Blake, W. H., Couldrick, L., Keith-roach, M. J. (2012). Sorption behaviour of
793 beryllium-7 and implications for its use as a sediment tracer. *Geoderma*, 187-188, 16–
794 23.

795 Taylor, A., Blake, W. H., Smith, H. G., Mabit, L., Keith-Roach, M. J. (2013). Assumptions
796 and challenges in the use of fallout beryllium-7 as a soil and sediment tracer in river
797 basins. *Earth-Science Reviews*, 126, *85-95*.

798 Thothong, W., Huon, S., Janeau, J.-L., Boonsaner, A., de Rouw, A., Planchon, O., Bardoux,
799 G., Parkpian, P. (2011). Impact of land use change and rainfall on sediment and carbon
800 accumulation in a water reservoir of North Thailand. *Agriculture, Ecosystems and*
801 *Environment*, 140(3-4), 521–533.

802 UNESCO (United Nations Educational Scientific and Cultural Organization). (1974).
803 FAO/UNESCO Soil map of the world, 1:5,000,000 Vol.1. Paris: UNESCO.

804 Valentin, C., Agus, F., Alamban, R., Boosaner, A., Bricquet, J. P., Chaplot, V., de Guzman,
805 T., de Rouw, A., Janeau, J.L., Orange, D., Phachomphonh, K., Podwojewski, P.,
806 Ribolzi, O., Silvera, N., Subagyono, K., Thiébaux, J.P., Vadari, T. (2008). Runoff and
807 sediment losses from 27 upland catchments in Southeast Asia: Impact of rapid land use
808 changes and conservation practices. *Agriculture, Ecosystems and Environment*, 128(4),
809 225–238.

Wallbrink, P. J., Murray, A. S. (1994). Fallout of ^{7}Be in South Eastern Australia. *Journal of Environmental Radioactivity*, 25(3), 213–228.

Walling, D. E. (2012). Beryllium-7: The Cinderella of fallout radionuclide sediment tracers? *Hydrological processes*, 27(6), 830–844.

Walling, D. E., He, Q. (1999). Using fallout lead-210 measurements to estimate soil erosion on cultivated land. *Soil Sci. Soc. Am. J.*, 63, 1404–1412.

Whiting, P. J., Matisoff, G., Fornes, W., Soster, F. M. (2005). Suspended sediment sources and transport distances in the Yellowstone River basin. *Geological Society of America Bulletin*, 117(3), 515–529.

Williams, G. P. (1989). Sediment concentration versus water discharge during single hydrologic events in rivers. *Journal of Hydrology*, 111, 89–106.

Yun-Liang, S., Wu, Y., Mei-E, R. (1985). Hydrological characteristics of the Changjiang and its relation to sediment transport to the sea. *Continental Shelf Research*, 4(1), 5–15.

Figure captions

Figure captions:

Fig. 1: Location of the Houay Xon catchment (top). Houay Xon S10 subcatchment sampling stations and main land uses areas during the study (centre). Location of surface soil, gully and riverbank samples, swamp areas and weather station (bottom).

Fig. 2: ^{7}Be, $^{210}Pb_{xs}$ and ^{137}Cs stock variations vs. total suspended sediment (TSS) concentration in overland flow exported from the 1-m² experimental plot during each of the 45 minutes of the June 1 event. Error bars represent 1σ uncertainty.

Fig. 3: Evolution of rainfall intensity, stream discharge (Q, thicker solid line), total suspended sediment (TSS) concentration, electric conductivity (EC), median particle size (d_{50}), ^{137}Cs, $^{210}Pb_{xs}$ and ^{7}Be activities and calculated percentage of fresh sediment (F; see text) at upstream station S1 (Houay Pano Stream) during the May 23 flood. River samples: grey circles. Error bars represent 1σ uncertainty.

Fig. 4: Evolution of rainfall intensity, stream discharge (Q, thicker solid line), total suspended sediment (TSS) concentration, electric conductivity (EC), median particle size (d_{50}), ^{137}Cs, $^{210}Pb_{xs}$ and ^{7}Be activities and calculated percentage of fresh sediment (F; see text) at intermediate station S4 (Houay Pano Stream) during the May 23 flood. River samples: grey circles. Error bars represent 1σ uncertainty.

Fig. 5: Evolution of rainfall intensity, stream discharge (Q, thicker solid line), total suspended sediment (TSS) concentration, electric conductivity (EC), median particle size (d_{50}), ^{137}Cs, $^{210}Pb_{xs}$ and ^{7}Be activities and calculated percentage of fresh sediment (F; see text) at downstream station S10 (Houay Xon River) during the May 23 flood. River samples: grey circles. Error bars represent 1σ uncertainty.

Fig. 6: Correlations between total suspended sediment (TSS) concentration and ^{7}Be activity at S1 (a) and S4 (b); c: relation between calculated percentage of fresh sediment (F) and calculated percentage of particles derived from surface soil (α) at S10 during the May 23 flood. Regression lines only consider black filled circles (c: peaks samples -white filled circles- are excluded from the regression). Error bars represent 1σ uncertainty.

Fig. 7: Evolution of stream discharge (Q, thicker solid line), total suspended sediment (TSS) concentration (small grey circles), calculated proportions of (1) particles derived from surface/subsurface soil (white/black pie chart) and (2) old/fresh sediment (light-grey/dark-grey pie chart) at S1 (a), S4 (b) and S10 (c) during each stage of the May 23 flood (rise-peak-recession).

Figure1

Click here to download high resolution image

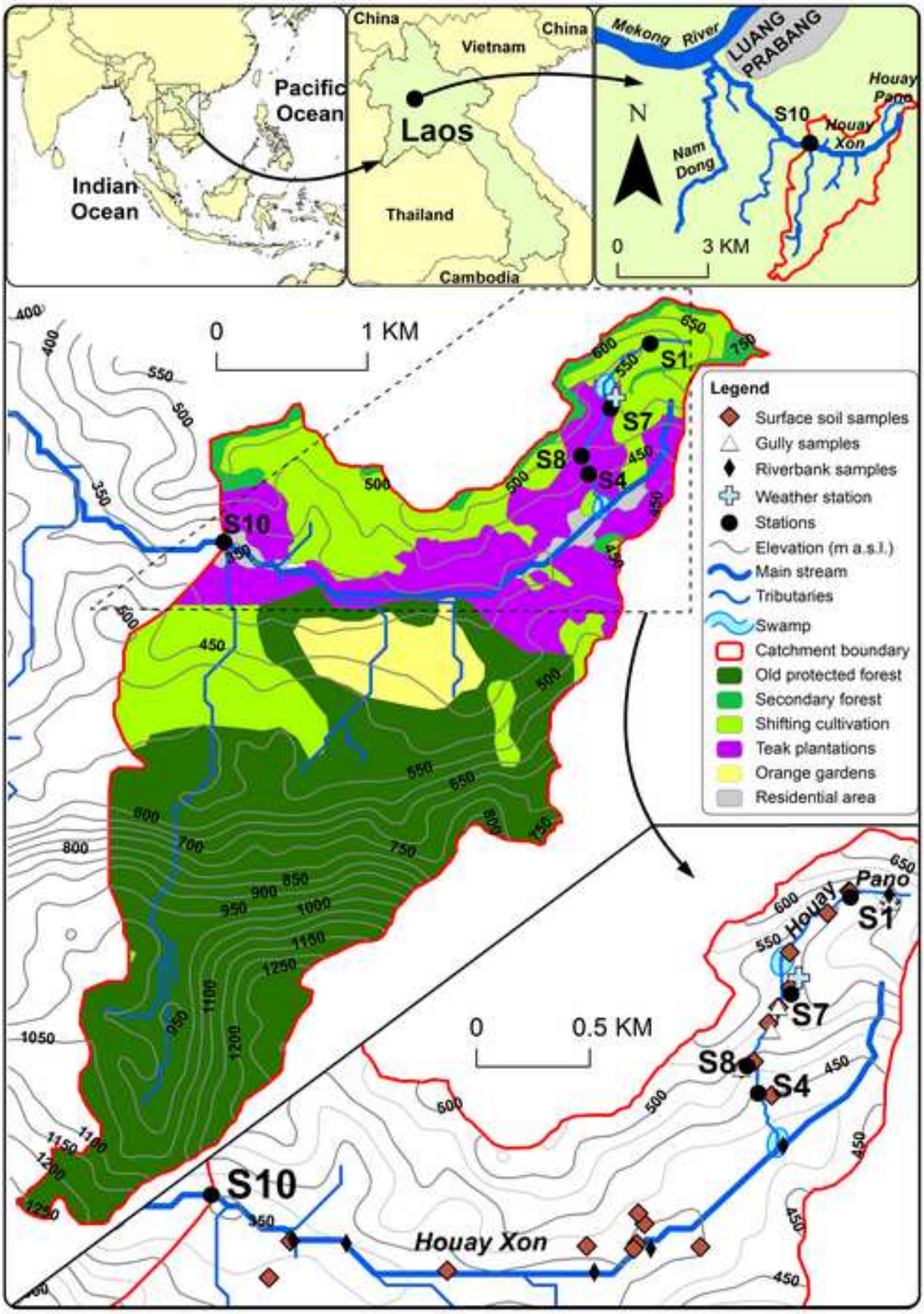

Figure2

Click here to download high resolution image

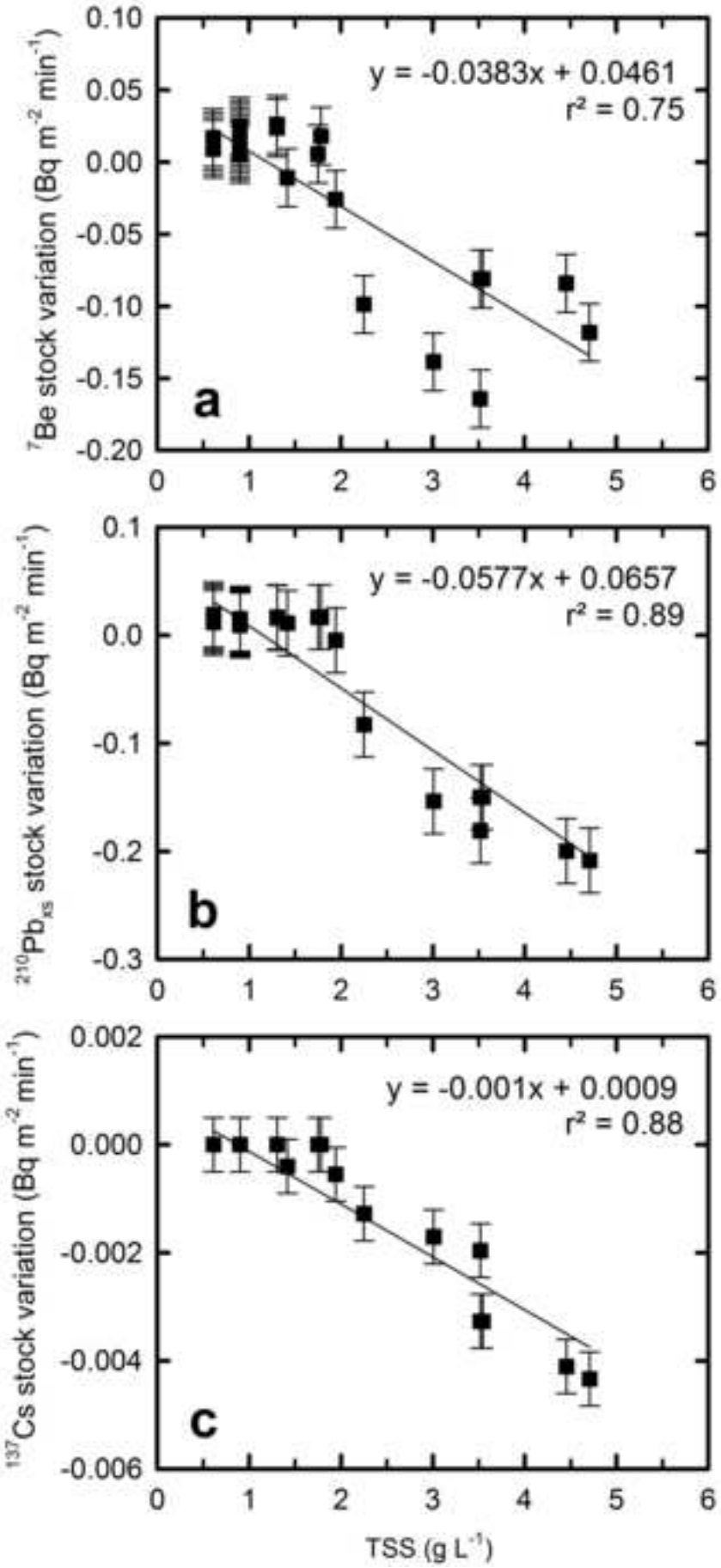

Figure3

Click here to download high resolution image

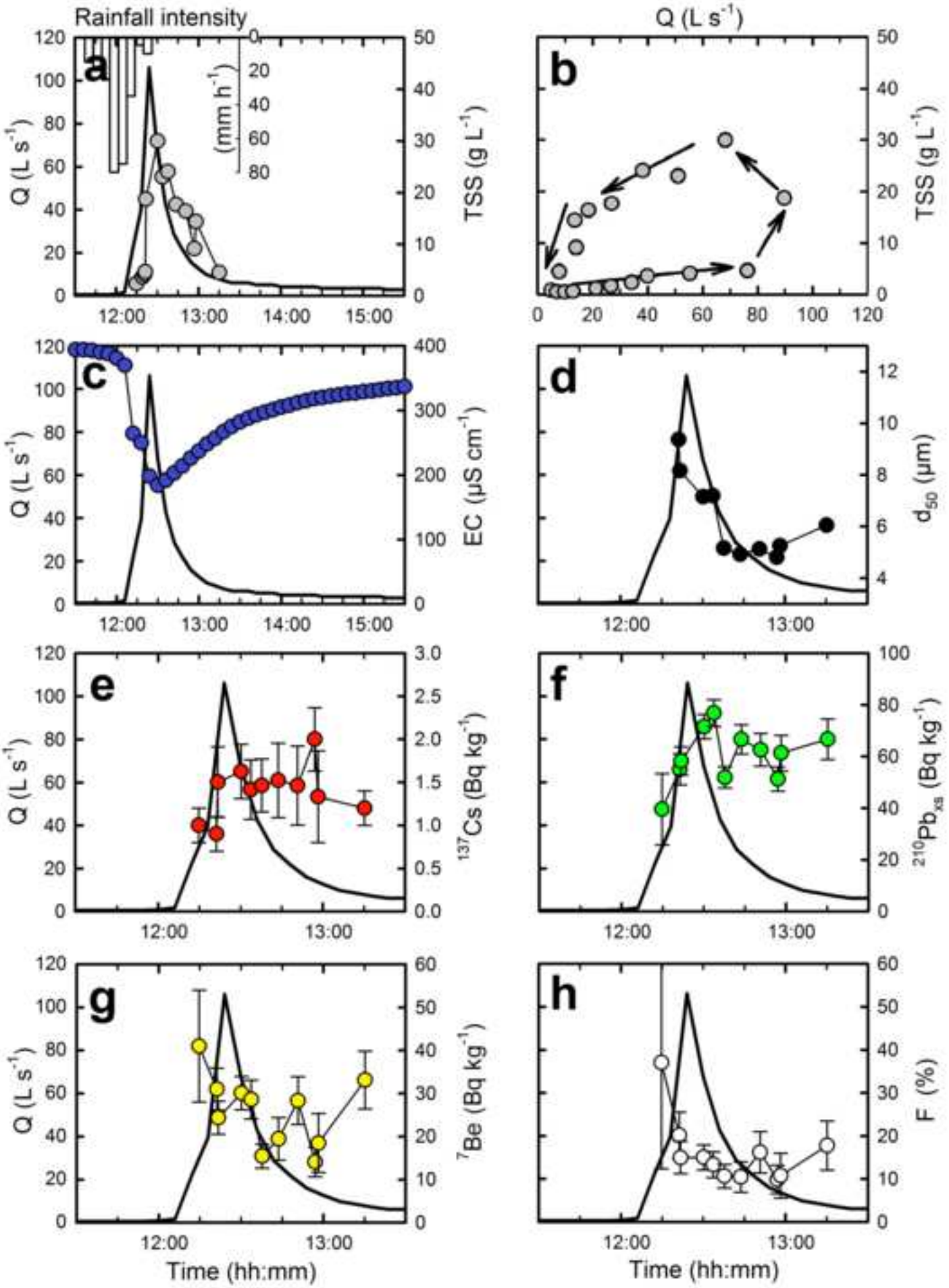

Figure4

Click here to download high resolution image

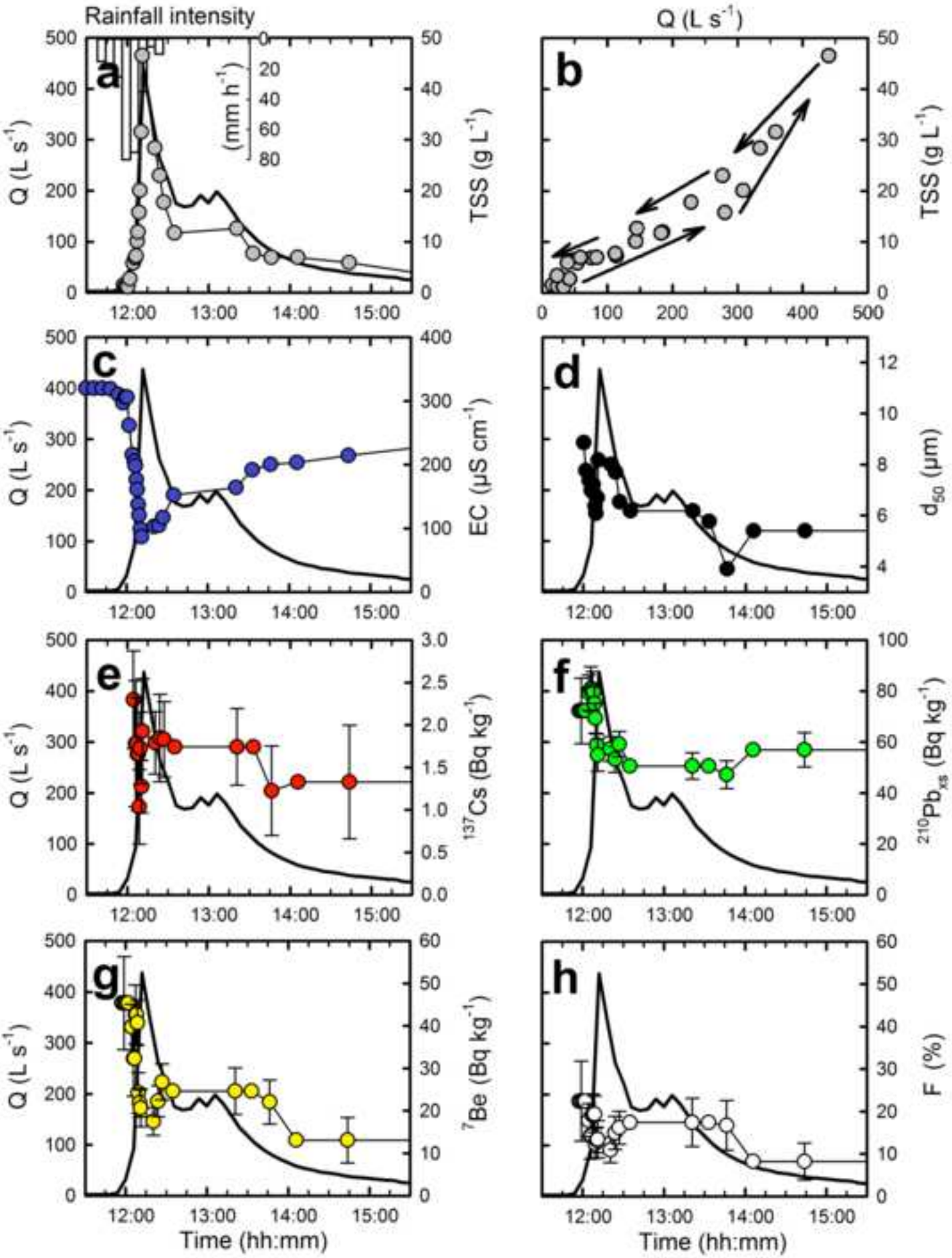

Figure5

Click here to download high resolution image

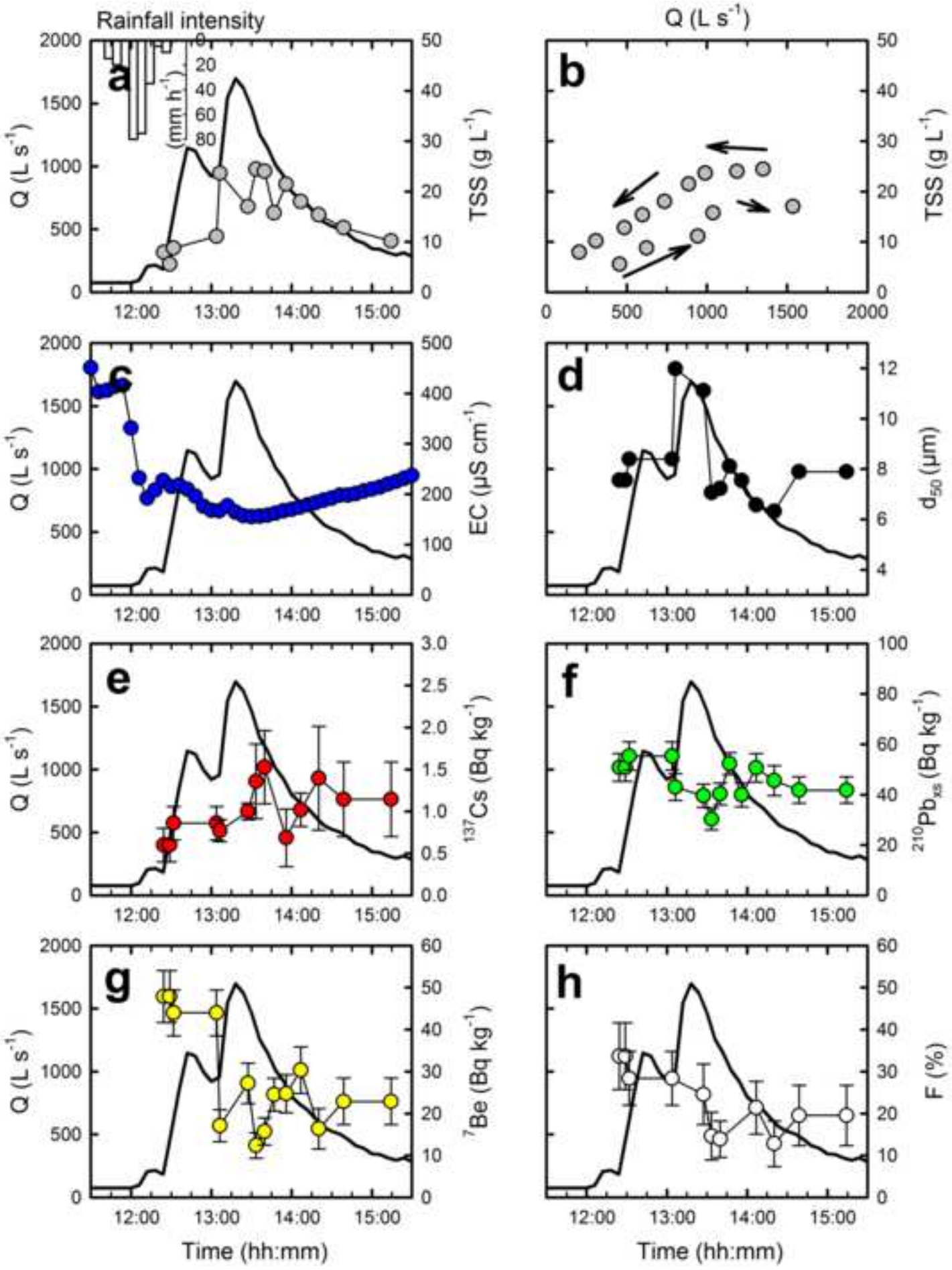

Figure6

Click here to download high resolution image

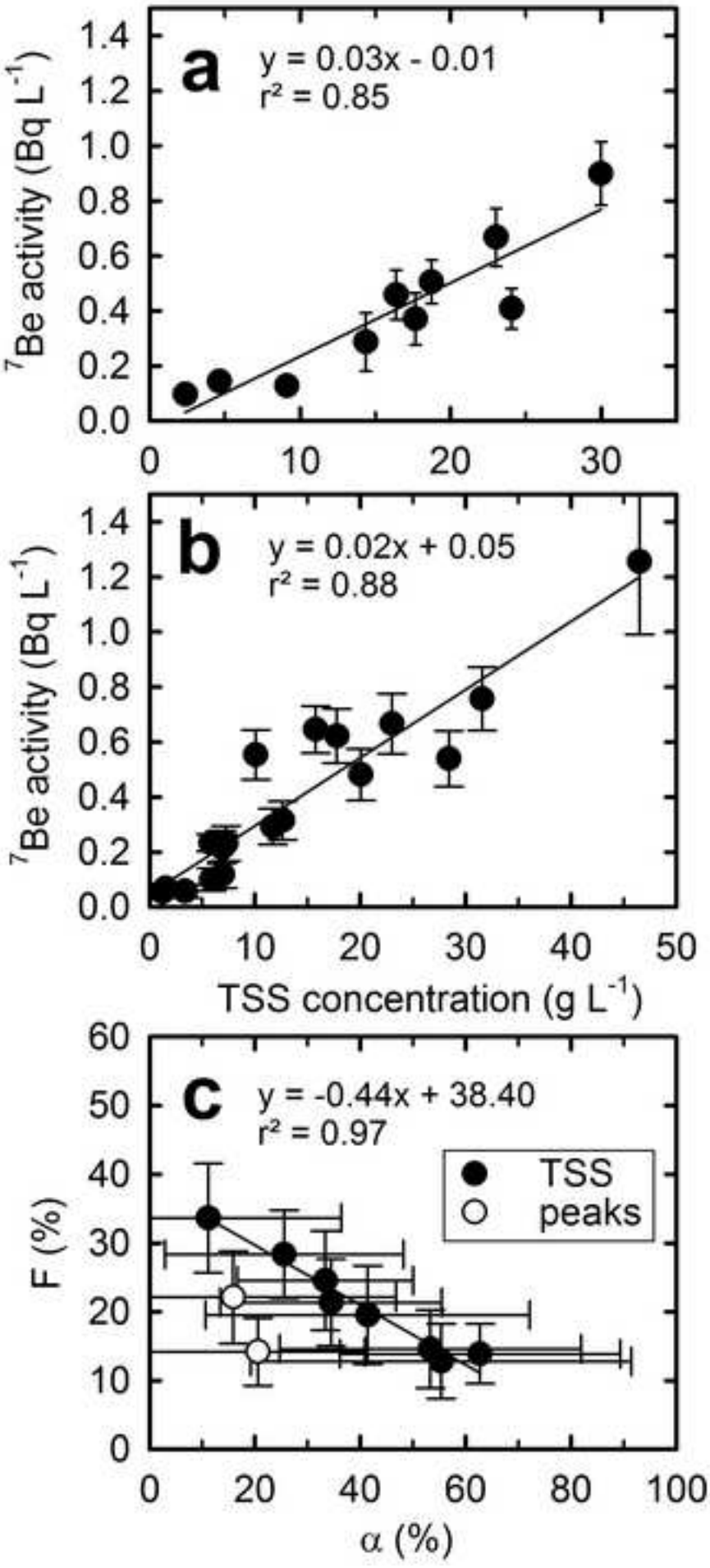

Figure7

Click here to download high resolution image

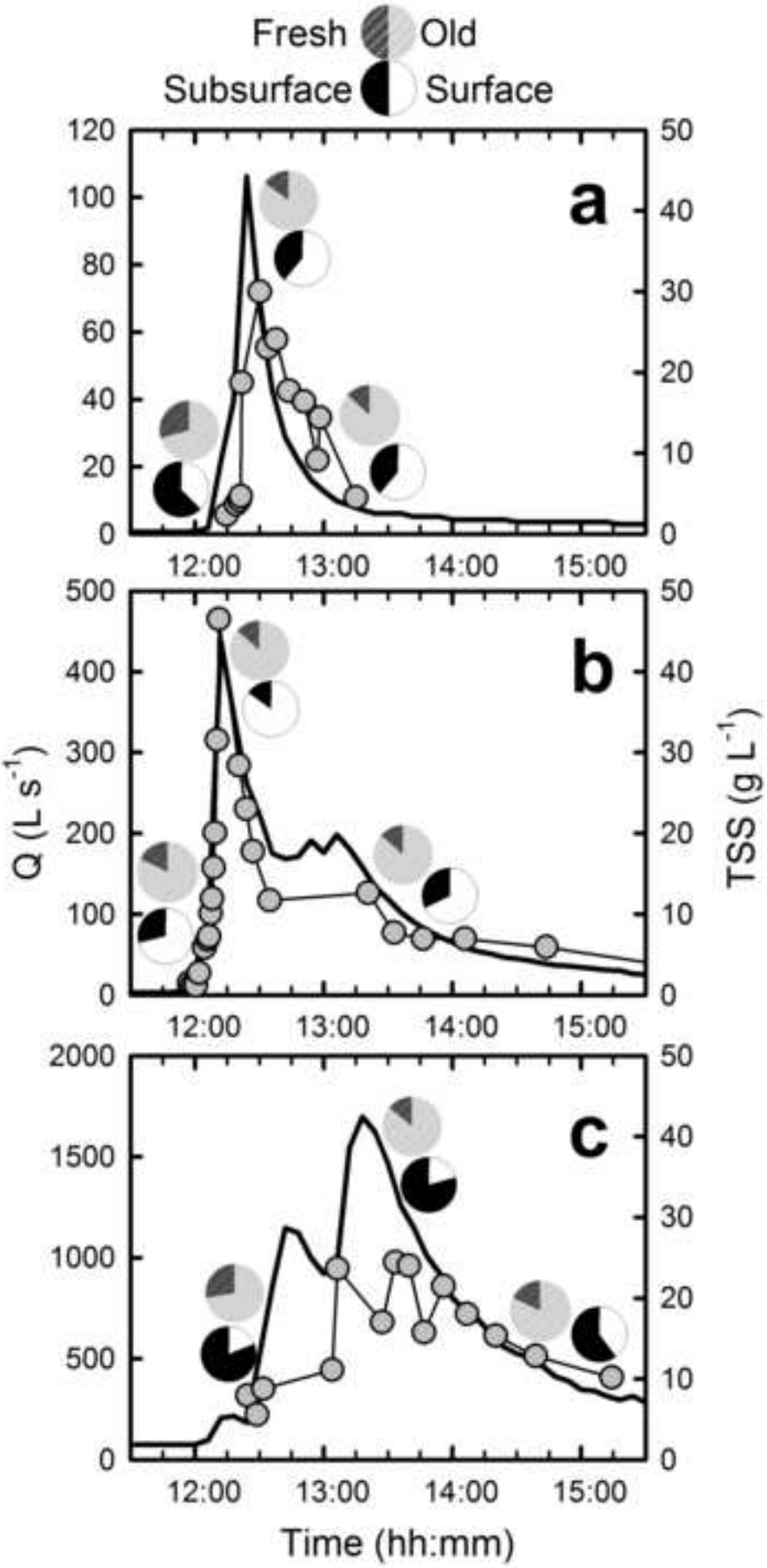

Table1

Click here to download Table: Table 1.doc

Table 1: Mean radionuclide activity (± 1 standard deviation) for surface soils, gullies and stream bank samples in the Houay Pano and Houay Xon catchments

Location	Number of samples	^{137}Cs (Bq kg^{-1})	$^{210}Pb_{xs}$ (Bq kg^{-1})
Surface soils*	65	2.2 ± 0.9	38 ± 19
Stream banks**	8	0.4 ± 0.3	14 ± 11
Gullies**	6	0.4 ± 0.3	21 ± 27

*Data from Huon et al. (2013) decay-corrected to 2012 and this study (2012), **this study (2012).

Table2

Click here to download Table: Table 2.doc

Table 2: Sediment budget for the May 23 flood event

Gauging station	S1	S4	S10
Suspended sediment exports (Mg)	2.3	26	130
Catchment surface (km^2)	0.20	0.60	11.6
Sediment yields (Mg km^{-2})	11.5	43.3	11.2

Table3
Click here to download Table: Table 3.doc

Table 3: Comparison of $^{7}Be/^{210}Pb_{xs}$ and estimates of fresh sediment proportion (F) compared to literature data

References	Location	Spatial scale	Temporal scale	$^{7}Be/^{210}Pb_{xs}$		F
				rainfall	sediment	
This study	Northern Laos	3 nested subcatchments (0.2-11.6 km²)	1 storm event	2.8	0.2 – 1.0	8 – 37 %
Evrard et al., 2010	Central Mexico	3 subcatchments (3 – 12 km²)	8 – 18 storms (6 months)	7- 27	2 – 14	10 – 80 %
Bonniwell et al., 1999	ID, USA	Catchment (390 km²) - River (*ca.* 30 km reach)	3 months	*n.a.*	0.3 – 3.8	18 – 96 %
Matisoff et al., 2005	OH; AL; OR, USA	3 catchments (70 km²)	Individual storms (1 year)	13 - 17	1.0 – 1.7	6 – 14 %
Huisman et al., 2013	WI, USA	Catchment (12.4 km²)	7 campaigns (6 months)	3 - 12	0.1 – 5.5	1 – 100 %

n.a. = not available

Supplementary material for on-line publication only

Click here to download Supplementary material for on-line publication only: Appendices.doc

Graphical Abstract (for review)